MDPI

Photocatalytic Degradation of Losartan with Bismuth Oxychloride: Batch and Pilot Scale Demonstration

Konstantinos Kouvelis [1], Alexandra A. Ioannidi [1], Athanasia Petala [2], Manolis Souliotis [3] and Zacharias Frontistis [3,*]

[1] Department of Chemical Engineering, University of Patras, GR-26504 Patras, Greece; koskouv@chemeng.upatras.gr (K.K.); alex.ioannidi@chemeng.upatras.gr (A.A.I.)

[2] Department of Environment, Ionian University, GR-29100 Zakynthos, Greece; apetala@ionio.gr

[3] Department of Chemical Engineering, University of Western Macedonia, GR-50132 Kozani, Greece; msouliotis@uowm.gr

[*] Correspondence: zfronistis@uowm.gr

Abstract: The solar-induced semiconductor photocatalytic process is one of the greenest and most promising technologies for the elimination of pharmaceuticals in aqueous media. In the context of this study, a bismuth oxychloride (BiOCl) photocatalyst was fabricated and characterized by its morphology, crystallographic structure, and optical properties. Its photocatalytic efficiency was tested towards the degradation of Losartan (LOS), a medication used to treat high blood pressure, in water using a solar simulator. The as-prepared BiOCl exhibited significant photocatalytic efficiency, achieving complete degradation of 0.3 mg/L LOS in short periods of irradiation (15–30 min). The examined system showed optimal efficiency using 500 mg/L of BiOCL (k_{app} = 0.21 min^{-1}) and pH 3 (k_{app} = 0.32 min^{-1}). However, LOS removal significantly decreased in environmentally relevant water matrices, including wastewater (k_{app} = 0.006 min^{-1}) and bottled water (k_{app} = 0.023 min^{-1}). Additional tests carried out in synthetic water matrices showed that the LOS degradation rate was reduced by more than 40% in the presence of humic acid (k_{app} = 0.016 min^{-1}) and bicarbonates (k_{app} = 0.029 min^{-1}), while chlorides did not affect the overall efficiency. Moreover, photogenerated holes and singlet oxygen were the dominant oxidative species. The efficiency of the BiOCl photocatalyst towards LOS degradation was further studied using a flat plate pilot-plant scale photoreactor. It was found that more than 75% of LOS was removed after 100 kJ/L of accumulated solar irradiation. The results obtained in the pilot-plant unit confirmed the suitability of BiOCl as a potential photocatalytic material.

Keywords: photocatalysis; advanced oxidation processes (AOPs); losartan; pilot-scale demonstration; bismuth oxychloride

1. Introduction

The insufficiency of conventional water treatment methods to eliminate a large number of chemical substances classified as emerging contaminants (ECs) has led to their detection not only in the effluents of wastewater treatment but also in surface water [1]. Their presence poses severe risks not only to the ecosystem but also to public health, thus leading many scientists to focus their efforts on developing new, more effective water treatment techniques [2]. In this context, advanced oxidation processes (AOPs) have shown very promising results. AOPs constitute a group of technologies based primarily but not exclusively on hydroxyl radicals ($^\bullet$OH) with a high oxidation potential for ECs degradation in water [3]. Hydroxyl radicals are characterized by non-selectivity and can be produced by various methods, enhancing AOPs' versatility and making them suitable for many wastewater treatment applications. Ozone, Fenton reagent, photocatalysis, and activated persulfate are some characteristic examples widely studied in ECs degradation systems [4].

In addition, hybrid systems, such as persulfate/photocatalysis [5] or a combination of cavitation with advanced oxidation processes [6], have enhanced oxidation efficiency.

If one had to choose the greenest technology among AOPs, photocatalysis would undoubtedly be the answer. This is because sunlight energy is used to activate the photocatalyst, usually a semiconductor, producing charge carriers that initiate chemical reactions for ECs degradation. As a result, water treatment by photocatalysis has been a topic of extensive research over the past three decades, resulting in an impressive number of papers in the area [7,8]. Especially nowadays, with sustainability gaining a prime position on the agenda of governments, highly efficient photocatalytic systems for wastewater treatment seem more necessary than ever. However, one of the main challenges in photocatalysis is translating fundamental research into practical applications. To increase the reported photocatalytic efficiencies, further research is needed towards both process optimization and photocatalyst development.

Undoubtedly, the lion's share among photocatalytic materials belongs to titanium dioxide (TiO_2) and its modifications [9–11]. However, in recent years, many researchers have focused their efforts on the development of non-TiO_2-based semiconductors. Among the many photocatalytic materials tested so far, bismuth-based photocatalysts such as $BiVO_4$ [12], Bi_2WO [13], Bi_2O_3 [14,15], BiOBr [16], and BiOCl [17] possess many desirable characteristics such as low cost and toxicity, high stability, and high photocatalytic activity. Bismuth oxychloride (BiOCl) belongs to the group of p-type semiconductors and has a band gap between 2.8 and 3.4 eV. It has demonstrated high efficiency in numerous energy and environmental applications [18]. This is primarily attributed to its layered structure and the suitable position of its energy bands. Numerous studies have reported its photocatalytic properties either in its pristine form or by doping it with metals/non-metals [19]. For instance, Gao et al. [20] presented the fabrication of BiOCl ultrathin nanosheets for carbamazepine photocatalytic degradation. They reported 91.1% carbamazepine removal after 30 min of simulated solar irradiation. Cobalt-doped BiOCl [21] was synthesized using a hydrothermal route and possessed significantly higher efficiency for Bisphenol A removal than pure BiOCl. Moreover, Shahid et al. [22] synthesized a Fe-modified BiOCl ultra-thin nanosheet with excellent efficiency for Cr (VI) and Rhodamine B photocatalytic degradation in water. In 2021, our group investigated sulfamethoxazole removal using BiOCl under simulated solar irradiation, emphasizing the water matrix effect on the overall efficiency [23]. In addition, valsartan removal was studied using MoS_2/BiOCl MoS_2 (0.1–10.0 wt.%) composite photocatalysts [24]. The results showed that 0.25 wt.% MoS_2/BiOCl was the best-performing photocatalytic material.

Although BiOCl has been used in many photocatalytic systems dealing with water remediation, no study has been carried out at the pilot-plant scale. Indeed, the majority of investigations in the heterogeneous photocatalysis area are in small laboratory setups irradiated with artificial light. However, the results obtained in lab installations are not very useful for practical applications as the experimental conditions are far from industrial ones.

In light of this, in the current work, BiOCl's efficiency was studied in (i) a batch reactor under simulated solar irradiation and (ii) in a pilot-plant demonstration using a stainless steel (SS) flat plate reflector (FPR), under solar radiation. For this, Losartan (LOS) removal was investigated. LOS is an angiotensin II receptor used for hypertension treatment. Among ECs, pharmaceuticals are receiving the greatest concern as their accumulation in water is linked to severe problems in public health. Unfortunately, the problem will continuously be magnified as pharmaceutical consumption shows an increasing trend worldwide. Indeed, a large amount of research during the COVID-19 pandemic revealed a significant increase in antibiotics and pharmaceutical consumption in general [25]. LOS degradation in aqueous media has rarely been studied using AOPs, resulting in promising results. Salazar et al. [26] reported LOS mineralization by electro-oxidation, while Ioannidi et al. [27] studied LOS removal utilizing heat-activated persulfate. Moreover, another study reported N-doped porous carbon as a peroxymonosulfate activator for LOS oxidation [28]. Considering LOS

removal in photocatalytic systems, only Guateque-Londoño et al. reported data considering LOS degradation using TiO_2-photocatalysis and UVC/persulfate (UVC/PS) [29].

In this context, the effect of BiOCl concentration and pH on LOS degradation was studied. The impact of the water matrix is highlighted with experiments in real (bottled water and wastewater) and synthetic (humic acid, bicarbonates, and chlorides) water matrices presented. Additional experiments were conducted by varying the irradiation type or by adding suitable radical scavengers. Finally, in order to collect data on the feasibility of BiOCl photocatalyst in practical applications, LOS degradation was tested in a stainless-steel (SS) flat-plate reflector (FPR).

2. Results and Discussion

2.1. BiOCl Characterization

XRD analyses (Figure 1) confirmed the successful preparation of the tetragonal BiOCl phase (JCPDS No 6-249) without impurities. In addition, the structural properties of the as-prepared BiOCl powder, as estimated by equations 1–4, are summarized in Table 1. The values of a and c were determined for planes <1 1 0> and <0 0 1>, respectively.
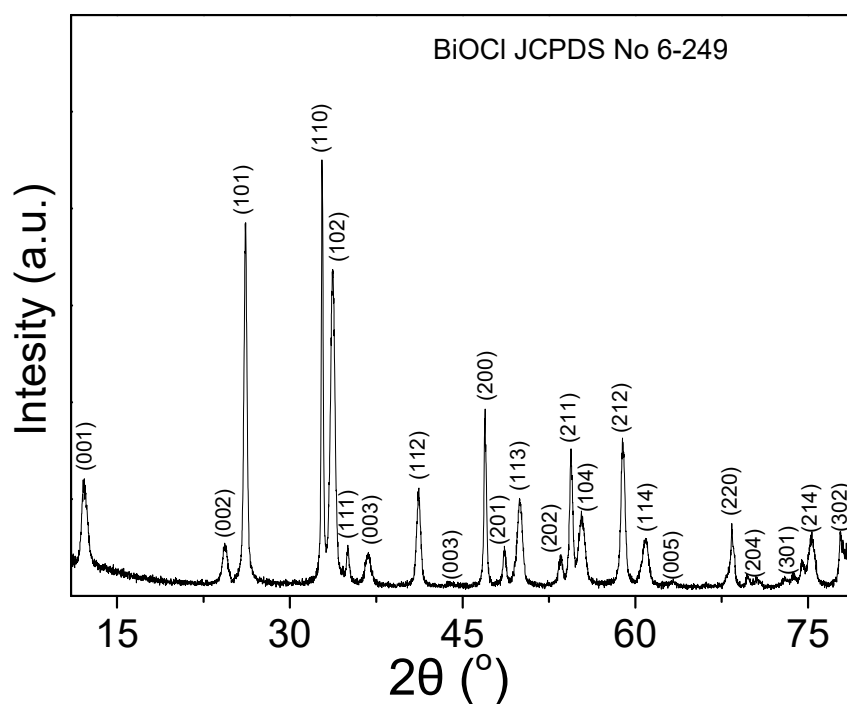

Figure 1. X-ray diffraction pattern of BiOCl.

Table 1. Structural properties of BiOCl.

Parameters	Values (Unit)
Lattice constant ($a = b$)	2.75 $\left(\text{Å}\right)$
Lattice constant (c)	7.39 $\left(\text{Å}\right)$
Unit cell volume (V)	55. 9 (Å^3)
Average crystallite size (D)	32.2 nm
Strain (ε) $\times 10^{-3}$	4.8

Moreover, the specific surface area of BiOCl was determined to ~16 $m^2 \cdot g^{-1}$ (Figure S1), in agreement with previous studies [30], while the total pore volume from the N_2 isotherms was found to be equal to 6.25 $cm^3 \cdot g$. In general, the specific surface area of BiOCl varies a

great deal from 3–50 m^2·g^{-1}, varying in the synthesis method. For example, Gao et al. [31] prepared BiOCl microspheres with a 13 m^2·g^{-1} surface area, while hydrothermally prepared BiOCl exhibited a ~7 m^2·g^{-1} surface area [32].

The optical characteristics of BiOCl were investigated utilizing diffuse reflectance spectroscopy (DRS). The inset in Figure 2 illustrates that the as-prepared BiOCl can absorb light with a wavelength of 450 nm or less. The sample's ability to absorb ultraviolet and visible light demonstrates the positive impact of thiourea alteration on the material's optical properties. Considering its band gap, it was found to be 2.5 eV using the Tauc diagram (Figure 2).
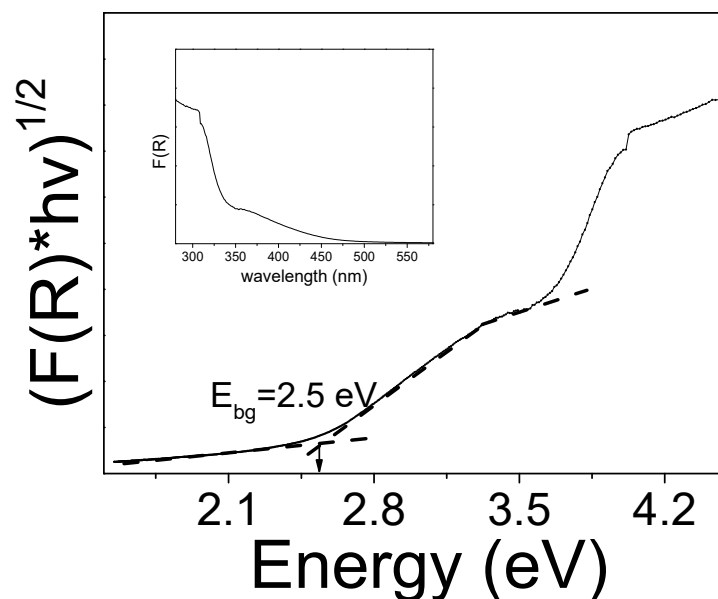

Figure 2. Tauc plot of BiOCl. Inset: Corresponding UV-vis diffuse reflectance spectrum.

Considering TEM analysis, Figure 3a,b shows that BiOCl comprises nanoplates with a thickness approximately equal to 12 nm. Notably, the margins of the nanoplates are composed of incredibly tiny spheres (Figure 3c). In addition, Figure 3d,e display typical SEM images with the energy-dispersive X-ray spectra, confirming the presence of Bi, O, and Cl alone.
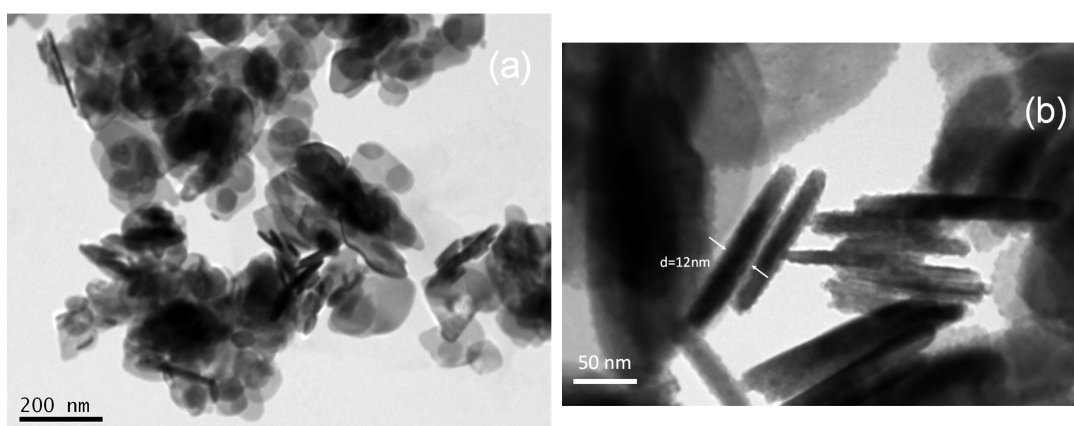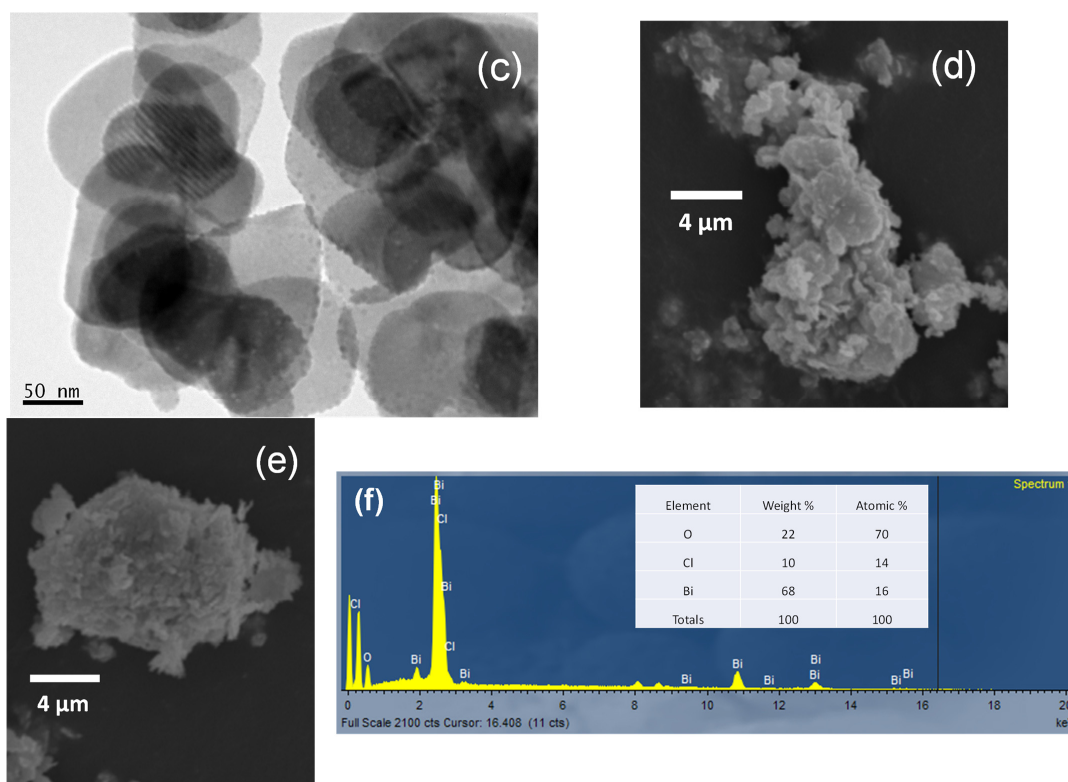

Figure 3. *Cont.*

Figure 3. (**a**–**c**) TEM and (**d**,**e**) SEM images of BiOCl. (**f**) EDS spectrum obtained from this SEM image.

The photocatalytic properties of BiOCl were investigated by assessing the transient photocurrent response of the as-prepared powder. In this regard, the fabricated FTO@BiOCl electrode was immersed in a 0.1 M Na_2SO_4 aqueous solution serving as the electrolyte. The experimental setup consisted of consecutive light on/off intervals, each lasting for 50 s. During these intervals, a constant external potential of 0.3 V was applied to the two-electrode system. According to Figure 4, photocurrent density values obtained under illumination equaled 0.18 $\mu A/cm^2$. Conversely, when the light source was switched off, the current value rapidly dropped to 0.08 $\mu A/cm^2$. This observation confirms the photocatalytic properties of the as-prepared material.
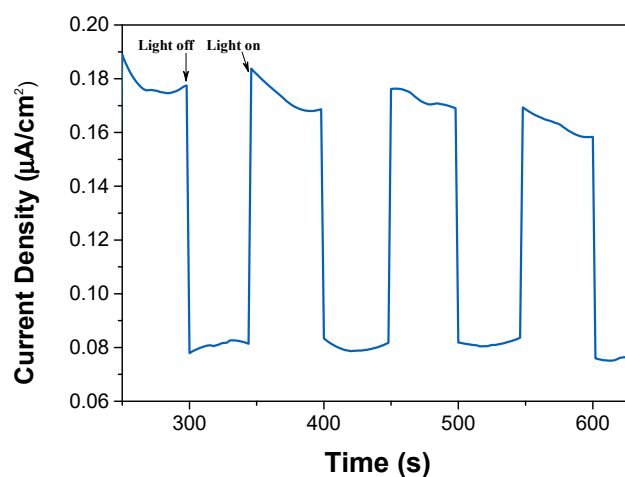
Figure 4. Transient photocurrent density of FTO@BiOCl at an applied potential of 0.3 V in a two-electrode system.

2.2. Effect of Operating Parameters on LOS Degradation

At the outset of the study, a methodical evaluation of the photocatalytic activity of BiOCl was undertaken to determine its efficacy in removing Losartan (LOS) from various aqueous matrices under solar irradiation. The primary aim was to identify the specific impact of various experimental parameters, including catalyst loading, the pollutant concentration, the pH level, and the complexity of the aqueous matrix, on photocatalytic efficiency. Additionally, we aimed to reveal the dominant reactive species of the system. The photocatalytic performance of BiOCl appears highly promising, leading to the complete removal of LOS within short experimental time frames, which is consistent with the findings of previous reports [23].

According to the literature, this type of photocatalytic system is adequately described by pseudo-first-order kinetics [33]. Specifically, the photocatalytic degradation rate can be expressed by the following equation,

$$\frac{dC}{dt} = -k_{app}C \rightarrow \ln\left(\frac{C}{C_0}\right) = k_{app}t \rightarrow \frac{C}{C_0} = e^{-k_{app}t} \tag{1}$$

where C and C_0 represent the LOS concentration (mg/L) at $t = t$ and $t = 0$, respectively.

The apparent kinetic constant (k_{app}) was calculated as the slope of the linear plot $\ln(C/C_0)$ vs. t (min), with k_{app} expressed in units of min^{-1}. The value of k_{app} is indicated in parentheses on each graph. The experimental data showed a strong fit to the previous kinetic model, with the coefficient of determination (R^2) values exceeding 0.98. The degradation percentage was estimated using the equation:

$$\text{Efficiency (\%)} = \frac{C_0 - C}{C_0} \times 100 \tag{2}$$

The effect of BiOCl concentration was identified by a set of experiments carried out, varying BiOCl loading between 125 and 500 mg/L in ultra-pure water (UPW). The obtained results are shown in Figure 5. As anticipated, increasing photocatalyst loading favors process efficiency by increasing the number of available active sites [34]. Specifically, the data collected at BiOCl loading levels of 250 and 500 mg/L were quite similar, and complete degradation of LOS was achieved under 30 min of irradiation. Conversely, with 125 mg/L BiOCl, the reaction rate was relatively low, as indicated by the significantly lower values of kapp (0.08 min^{-1}).
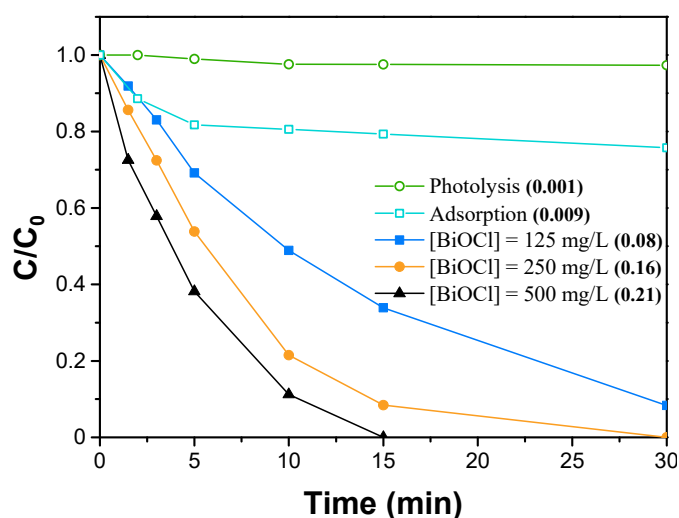

Figure 5. Effect of BiOCl loading in the range between 0 and 500 mg/L towards LOS (0.3 mg/L in UPW) degradation under simulated solar irradiation. Apparent rate constants (k_{app}) are presented in brackets in min^{-1}.

To quantify the impact of photolysis, additional tests were carried out in the absence of BiOCl. As shown in Figure 5, photolysis can be considered negligible since LOS removal did not exceed 5% under solar irradiation alone. This finding agrees with Kollipara et al., who highlighted the notable stability of LOS under photolytic stress conditions [35]. Additionally, a control experiment conducted in the dark for 30 min revealed that LOS removal due to adsorption phenomena was less than 20%, in line with previous results [16].

Maintaining an appropriate pH level in the dispersion is critical for the success of a photocatalytic process. The surface charge of the photocatalyst is strongly dependent on the pH level of the solution and influences the interactions with the pollutant molecules. Moreover, pH can alter the nature of the organic compound (LOS) and the elimination mechanism [36].

The role of pH in photocatalytic efficacy was elucidated by adjusting the solution pH at three distinct values: Acidic (pH 3), neutral (inherent pH), and alkaline (pH 9). The results of these experiments are demonstrated in Figure 6a. Remarkably, optimal degradation efficiencies were observed at pH 3, where complete elimination of LOS was achieved within 10 min of irradiation. Conversely, at pH 9, the degradation rate significantly slowed, resulting in a five-fold decrease in k_{app}. A possible explanation for the observed results is the variation in the surface charge of BiOCl, as a function of pH, in conjunction with the prevailing form of LOS. Specifically, LOS has a reported pKa value of 5.5 [37]. At pH 3, LOS exists in a cationic form and likely attracts the negatively charged BiOCl surface, facilitating LOS transfer to the catalyst surface. In contrast, at pH 9, slight deprotonation of LOS molecules may occur, leading to potential repulsive interactions between the organic compound and the photocatalyst.
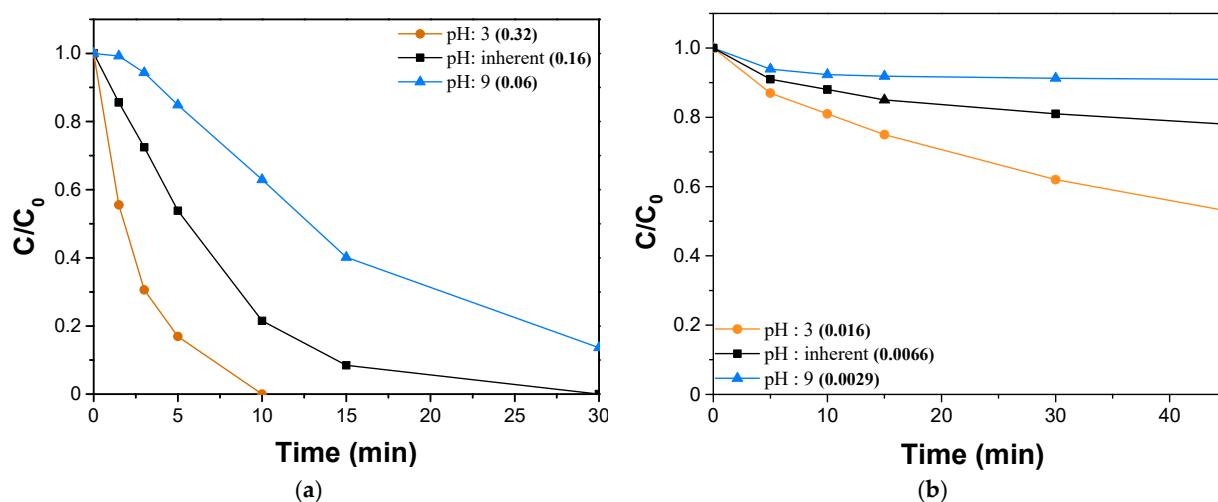

Figure 6. (**a**) Influence of initial solution pH (3, inherent, 9) on LOS photodegradation with 250 mg/L BiOCl in UPW. (**b**) Adsorption of 0.3 mg/L LOS with 250 mg/L BiOCl in three distinct pH levels (3, inherent, 9).

To acquire a more comprehensive understanding of the interactions at the LOS–BiOCl interface, additional experiments were conducted in the dark at the aforementioned pH values. The results are displayed in Figure 6b. Consistent with previous results, the highest LOS removal is achieved at pH 3, confirming the favorable interactions between the photocatalyst and the pollutant under these conditions. Conversely, at pH 9, adsorption was practically zero, highlighting the limitations of the LOS molecule's ability to reach the BiOCl surface.

Despite the extensive study of photocatalysis for the degradation of organic pollutants, its efficiency under realistic conditions remains mediocre. These limitations largely arise from the complexity of water environments, which include a variety of inorganic salts and organic matter [38].

Therefore, the impact of the water matrix was assessed by performing a series of tests using representative samples of BW and WW. The results are shown in Figure 7a. It is evident that the degradation rate of LOS was significantly reduced in BW, with the apparent rate constant decreasing nearly tenfold (0.023 min^{-1}) compared to UPW. These retarding phenomena are further amplified in the case of WW, resulting in a decomposition of LOS below 20%.
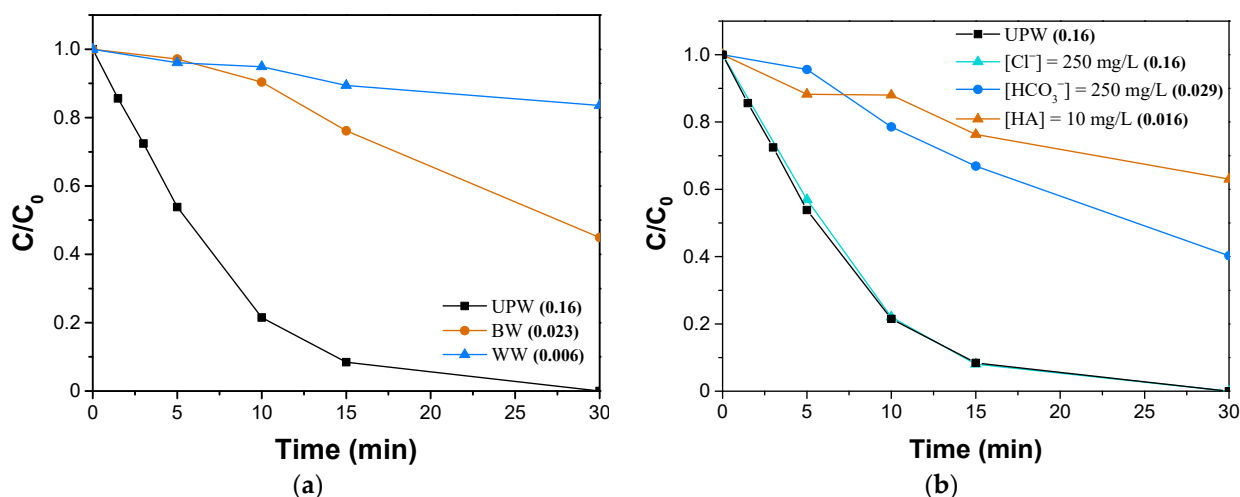
Figure 7. (**a**) Effect of water matrix complexity on the degradation of 0.3 mg/L LOS using 250 mg/L BiOCl in UPW. (**b**) Effect of HA (10 mg/L), HCO$_3^-$ (250 mg/L), and Cl$^-$ (250 mg/L) on the removal of 0.3 mg/L LOS employing 250 mg/L BiOCl.

The decreased removal efficiencies in BW and WW can be directly associated with the presence of diverse ions. These ions can act as quenchers of the photogenerated hydroxyl radicals ($^\bullet$OH) and/or may even instantly capture holes from the photocatalyst's surface [39,40]. Furthermore, in the case of WW, light penetration through the suspension is quite limited, leading to the adsorption of an insufficient number of photons on the photocatalyst surface [38]. At the same time, since photocatalytic degradation is a heterogeneous process in which most oxidation reactions occur on or near the solid/liquid interface, competition also exists between the pollutant, natural or effluent organic matter, and inorganic ions for adsorption on the catalyst surface. As already discussed in the section concerning the impact of pH, LOS adsorption was not favored under alkaline conditions, thus slowing down the performance in the real matrices evaluated where the pH ranged from 7.5 to 9.

In conclusion, the previous experiments revealed the presence of retarding phenomena attributed to the presence of ions and organic matter in aqueous media of environmental concern. These findings highlight the detrimental effect of increased water matrix complexity on the photocatalytic process.

To gain deeper insight into the influence of the water matrix, the efficiency of the present system was tested in synthetic matrices obtained by adding humic acid (HA, 10 mg/L), bicarbonates (BIC, NaHCO$_3$, 250 mg/L), and sodium chloride (NaCl, 250 mg/L) to UPW. Specifically, HA was selected as a typical agent of the organic matter found in environmental samples, while BIC and NaCl are the prevalent anions in BW. The experimental results, summarized in Figure 7b, revealed the hindering role of HA in the photocatalytic process, as the photocatalytic degradation efficiency was reduced by approximately 40%. HA can compete with the target pollutants for adsorption onto the photocatalyst surface and act as a barrier, obstructing light penetration [38,41]. Similar results were observed using 250 mg/L NaHCO$_3$, where a significant sixfold reduction of the k$_{app}$ (compared to UPW) was observed. This adverse impact is likely related to BIC's potential quenching of the reactive species, leading to the formation of radicals with lower oxidation potential (CO$_3^{\bullet-}$) [42,43]. In contrast, the presence of NaCl had negligible effects on the process, as it did not induce any noticeable changes in the k$_{app}$ value.

2.3. Effect of Type of Irradiation on the Degradation of LOS

One of the primary challenges in photocatalysis is to develop suitable photocatalytic materials capable of harnessing the visible section of the solar spectrum. The majority of conventional photocatalysts utilize only ultraviolet (UV) light, which constitutes only 5% of the total solar radiation; as a result, a significant fraction of solar energy remains unexploited [44,45].

To specifically assess the contribution of visible light, a 420 nm cut-off filter was utilized, which selectively blocks wavelengths below 420 nm. As depicted in Figure 8, the results indicate that nearly 60% of the LOS degradation can be attributed to visible light alone, compared to the complete degradation achieved utilizing the full solar spectrum. Notably, the calculated k_{app} value shows a tenfold decrease under visible light conditions (0.017 min^{-1}), confirming the limited response of BiOCl to visible light [46].
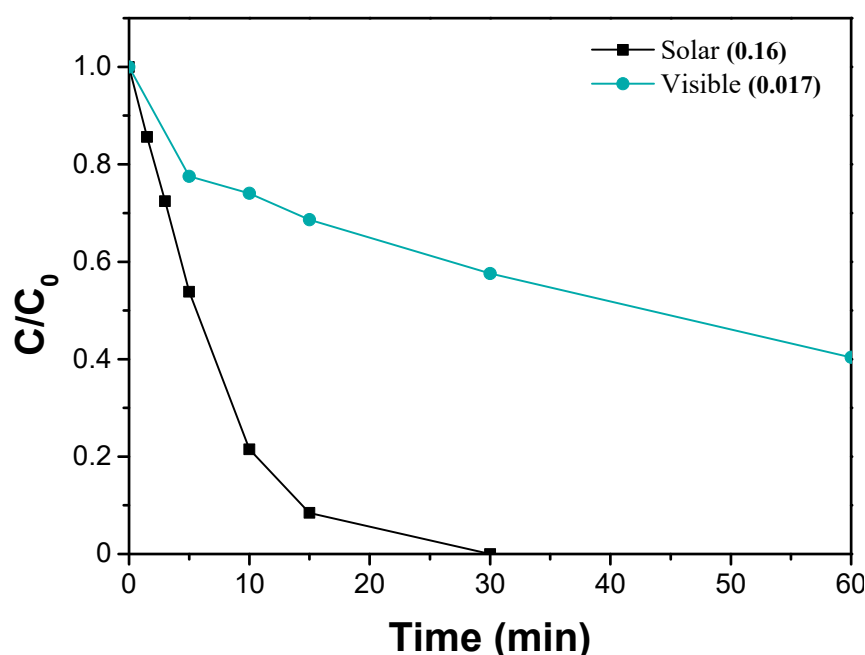
Figure 8. Degradation of 0.3 mg/L LOS using a 420 nm cut–off filter to isolate visible light. Experimental conditions: [BiOCl] = 250 mg/L, inherent pH, UPW.

2.4. Photocatalytic Mechanism

Subsequently, the dominant oxidizing species present in the solution was identified by trapping experiments. In this regard, tert-butanol (t-BuOH, 9.24 mM) was employed as a scavenger of $^{\bullet}$OH [47], sodium azide (NaN$_3$, 9.24 mM) was used to quench singlet oxygen (^{1}O$_2$) [48], and oxalic acid (C$_2$H$_2$O$_4$) was utilized to capture photo-induced holes (h$^+$) [49]. It was observed that the addition of 9.24 mM t-BuOH did not affect LOS degradation, indicating the possible absence of $^{\bullet}$OH in the solution (Figure 9). In contrast, in the presence of 9.24 mM NaN$_3$ or C$_2$H$_2$O$_4$, the degradation rate was completely inhibited, and the LOS concentration remained constant even after 30 min of irradiation. These findings strongly support the existence of both ^{1}O$_2$ and h$^+$, suggesting their substantial contribution to the efficient elimination of 0.3 mg/L LOS.
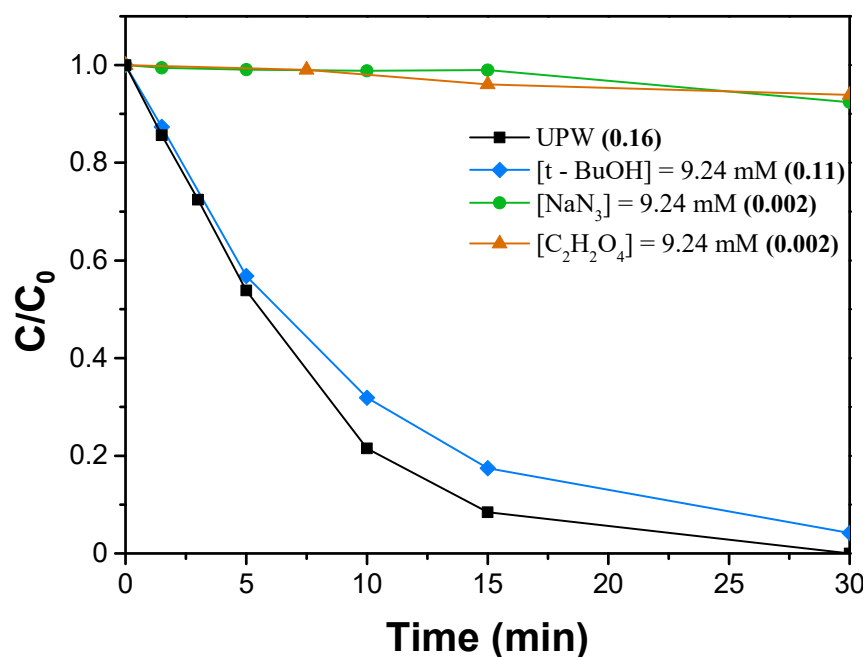
Figure 9. Effect of radical scavengers on the degradation of 0.3 mg/L LOS in UPW. Experimental condition: [BiOCl] = 250 mg/L, [Scavengers] = 9.24 mM.

Based on the above findings, the LOS degradation mechanism can be reported as follows: Photo-generated holes have the ability to directly oxidize the organic compounds (LOS) into smaller molecules, while the excited electrons (e−) in the conduction band (CB) of BiOCl can reduce the adsorbed oxygen, thus forming superoxide radicals ($O_2^{\bullet-}$).). Subsequently, $O_2^{\bullet-}$ can undergo further oxidation to generate $^1O_2$. Alternatively, adsorbed oxygen can be directly excited to $^1O_2$ [50]. $^1O_2$ exhibits strong oxidizing properties and is capable of oxidizing unsaturated organic compounds, including LOS and its intermediates [51]. Although the identification of LOS degradation by-products was not within the scope of this work, an additional experiment was performed at a higher LOS concentration, and the total organic carbon was monitored, as depicted in Figure S2. It is evident that the TOC removal only reached 40% after 180 min, which is significantly lower than the LOS removal measured by liquid chromatography, indicating the generation of LOS transformation products.

2.5. Photocatalyst Reusability

In the final phase of the study, the stability and reusability of BiOCl were assessed through a series of five consecutive tests. In each test, a dosage of 250 mg/L BiOCl was utilized for 0.3 mg/L LOS degradation in UPW. After each run, BiOCl powder was recovered through vacuum filtration and dried at 60 °C overnight to remove residual moisture.

Remarkably, BiOCl revealed notable stability throughout the consecutive tests, consistently maintaining its efficacy in achieving 100% elimination of LOS after 30 min of irradiation, as can be noted in Figure 10. These findings highlight the durability and reusability of BiOCl, affirming its potential application under realistic conditions.
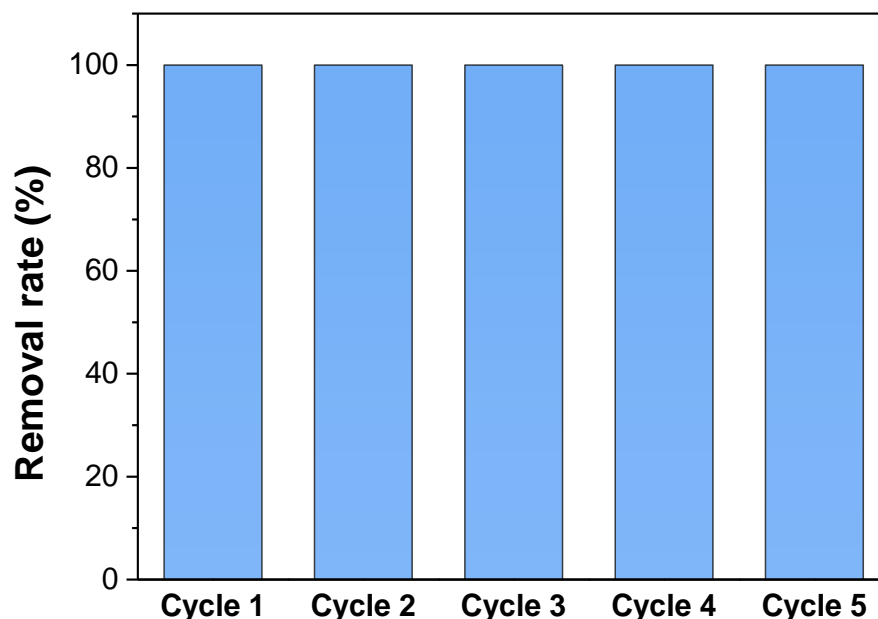
Figure 10. Reuse efficiency of BiOCl employing 250 mg/L and an initial concentration of 0.3 mg/L LOS in UPW.
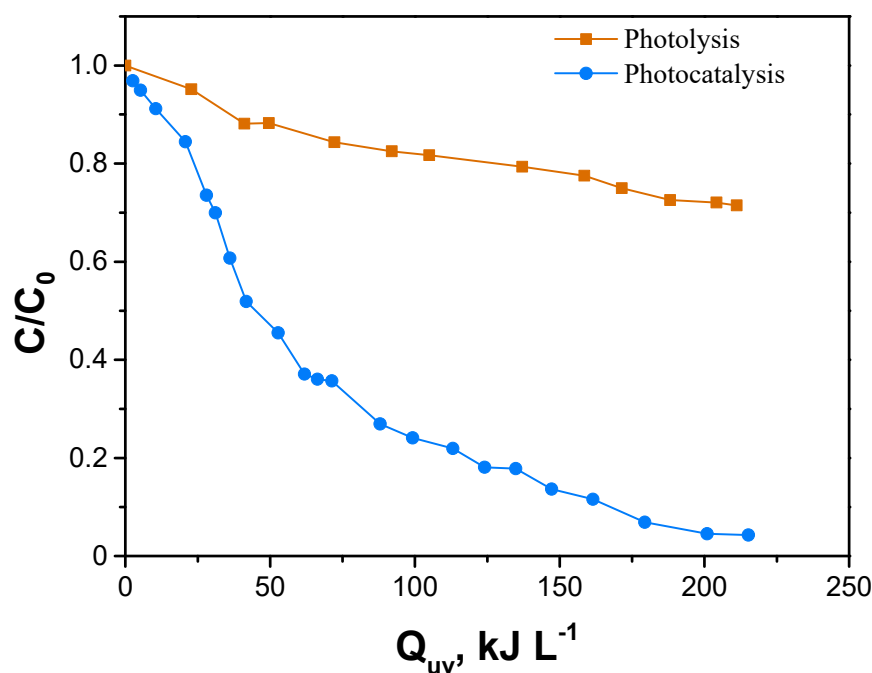
2.6. Pilot-Plant Scale Photoreactor

In the second stage, we decided to examine the scaling up of the BiOCl photocatalyst, employing a stainless-steel (SS) flat-plate reflector (FPR). The photoreactor configuration consisted of eight borosilicate tubes with an outer diameter of 32 mm, complemented by a tank with a working volume of 35 L and a centrifugal pump. A comprehensive description of the installation can be found elsewhere [52].

In particular, considering the results obtained from lab-scale batch reactors and the literature regarding photocatalytic oxidation experiments in solar-light pilot-plants, suitable experimental parameters were selected (250 mg/L BiOCl and 0.3 mg/L LOS) [53]. It is worth noting that increasing photocatalyst (BiOCl in this case) loading beyond a certain limit might lead to light obstruction phenomena due to the development of turbidity [53].

Concerning the experimental process, the reactor was covered and kept in the dark for 15 min to allow adsorption–desorption reactions to reach equilibrium. Subsequently, the reactor was exposed to sunlight, thereby initiating the photocatalytic process. To account for variations in the UV intensity on different days, the photodegradation of the pollutant in the SS pilot-scale photoreactor was expressed as a function of the accumulated UV energy Q_{uv} (kJ/L). As shown in Figure 11, there was a significant (almost 60%) removal of LOS after 50 kJ/L of irradiation. However, the degradation rate gradually decreased, and an almost complete elimination of LOS was eventually achieved near 200 kJ/L of accumulated irradiation. Additionally, photolysis accounted for less than 30% of total LOS degradation during the same solar energy.

In summary, this was an important first step towards upscaling the photocatalytic process using an easy-to-implement installation. The results were promising, as the organic compound was completely decomposed. Further research should focus on determining the optimal photoreactor geometry, aiming to ensure sufficient light distribution and harness a larger fraction of the incident radiation. Additionally, the optimization of the operational parameters, including the flow rate and catalyst loading, is crucial for enhancing treatment performance.

Figure 11. Degradation of LOS (C_0 = 0.3 mg/L) as a function of Q_{UV} (kJ L^{-1}) in SS pilot–scale photoreactor under natural sunlight. Experimental conditions: [BiOCl] = 250 mg/L, DW.

3. Materials and Methods

3.1. Chemical and Water Matrices

Bismuth (III) nitrate pentahydrate ($Bi(NO_3)_3 \cdot 5H_2O$, CAS No:10035-06-0), acetic acid (CH_3COOH, CAS No:64-19-7), and potassium chloride (KCl, CAS No:7447-40-7) used for the photocatalyst's synthesis were supplied by Sigma-Aldrich. Ethylene glycol ($HOCH_2CH_2OH$, CAS No:107-21-1) and thiourea (CH_4N_2S, CAS No:62-56-6) were supplied by Alfa Aesar.

The pharmaceutical Department of the University of Patras supplied us with Losartan (LOS, $C_{22}H_{23}ClN_6O$, CAS No:114798-26-4)

The primary characteristics of the water samples utilized in this study are as follows: (a) Bottled water (BW): conductivity = 0.39 mS/cm, alkalinity = 152 mg/L, pH = 7.5, 10 mg/L Cl^-, 5 mg/L SO_4^{2-}, 6.5 mg/L NO_3^-, 300 mg/L HCO_3^-; (b) secondary treated wastewater (WW): Conductivity = 0.33 mg/L, total suspended solids = 2 mg/L, alkalinity = 190 mg/L, pH = 8, chemical oxygen demand = 23 mg/L, total organic carbon = 8 mg/L, total suspended solids = 2 mg/L; (c) ultrapure water (UPW): Conductivity: 0.012 mS/cm, pH = 6.

3.2. Photocatalyst Synthesis and Characterization

For the synthesis of BiOCl, 100 mL of an ethylene glycol/water solution (1:1 *v/v* ratio) was first prepared. The aforementioned solution was subjected to stirring with the addition of Bi (NO_3)$_3 \cdot 5H_2O$ (4.85 g). After 1 h, the addition of 10 mL of a thiourea solution (CH_4N_2S 1.0 mol/L) and 0.01 mol KCl took place. The final step included the dropwise addition of a 2% (*v/v*) CH_3COOH solution (100 mL) and stirring for another 1 h. Vacuum filtration was used to separate the as obtained material, which was then dried at 70 °C for 12 h. More details can be found elsewhere [23,54].

XRD analysis was carried out with a Brucker D8 Advance (Cu Kα) device (Billerica, MA, USA), and crystallographic phases were identified using JCPDS cards. For the determination of the specific surface area of BiOCl, the Brunaueur–Emmett–Teller (BET) method (N_2 physisorption at the temperature of liquid nitrogen (77 K)) was adapted (Micromeritics, Gemini III 2375, Norcross, GA, USA). SEM images were recorded with a JEOL 6300 (JEOL USA, Inc., Peabody, MA, USA) microscope, while TEM images were obtained with an Erlangshen CCD Camera (Gatan Model 782 ES500 W, Pleasanton, CA, USA). Details can be

found elsewhere [54]. The diffuse reflectance spectrum (DRS) of BiOCl was obtained with a Varian Cary 3 UV-vis spectrophotometer. Its optical band gap was evaluated based on the following expression [55,56]:

$$(\alpha h\nu)^{1/n} = B\left(h\nu - E_{bg}\right) \tag{3}$$

where α is the absorption coefficient, $h\nu$ is the incident photon energy, E_{bg} is the band gap energy, B is a constant related to the effective masses of charge carriers associated with valance and conduction bands, and n is a factor that depends on the kind of optical transition induced by photon absorption.

The average size of crystallites, denoted by D, was estimated utilizing Debye–Scherrer's formula. The formula is expressed as follows [45]:

$$D = \frac{0.9\,\lambda}{\beta\,cos\theta} \tag{4}$$

where:

D represents the average crystallite size.
λ corresponds to the wavelength of the X-rays used.
β indicates the full width at half maximum (FWHM) of the diffraction peak.
θ represents the diffraction angle.

The lattice constants ($a = b$, c) of the tetragonal system, unit cell volume (V), and strain (ε) were all determined according to Equations (3)–(5) [57,58]:

$$\frac{1}{d^2} = \frac{h^2}{a^2} + \frac{k^2}{b^2} + \frac{l^2}{c^2} \tag{5}$$

where:

d represents the interplanar spacing.
h, k, and l are the Miller indices.

$$V = a^2 c \tag{6}$$

$$\varepsilon = \frac{\beta}{4tan\theta} \tag{7}$$

3.3. Photoanode Fabrication

Thin BiOCl films were deposited on fluorine–doped tin oxide (FTO)-coated glass for the chronoamperometry experiments. FTO substrates were chosen for their high conductivity, rendering them suitable for electrochemical experiments. Moreover, the optical transparency of FTO allows the illumination of the sample, which is essential in photocurrent response experiments. Initially, a mixture was prepared by combining 100 mg/L BiOCl, 1.2 mL of ethanol, and 0.4 mL of Nafion. The mixture was then ultrasonicated (ultrasonic bath Bandelin Sonorex RK 100 operated at 35 kHz, Bandelin electronic GmbH & Co. KG (Berlin, Germany)) for 30 min similar to the work of Wang J. et al. 2019 [59]. Nafion was employed to enhance the stability of the electrode and improve the uniformity of the thin film. The resulting yellowish suspension was drop-casted onto the FTO glass surface and then dried overnight at 75 °C. The electrode had a surface area of 1×1 cm^2 with an areal density of 3 mg/cm^2.

3.4. Photocatalytic Degradation Experiments

In a typical experiment, an appropriate quantity of photocatalyst (250 mg/L) was introduced into 120 mL of ultrapure water (UPW) containing 0.3 mg/L of LOS. The mixture was then stirred in the dark for 15 min to attain the adsorption–desorption equilibrium. A

solar simulator (Oriel, model LCS-100) equipped with a 100 W xenon ozone-free lamp was utilized as the light source, providing an incident intensity of 1.3×10^{-4} einstein/(m^2·s). At predetermined time intervals, a 1.2 mL sample was withdrawn. Subsequently, the samples were filtered through a PVDF Whatman Uniflo Syringe Filter featuring a polypropylene overmold housing (0.22 μm, Whatman, UK), and the resulting filtrate was analyzed using liquid chromatography.

In the recycle/reusability experiments, after each cycle, the catalyst was gathered, filtered, and rinsed multiple times with deionized water. Subsequently, it was dried overnight at a temperature of 60 °C and utilized in the subsequent cycle.

3.5. Chronoamperometric Measurements

The transient photocurrent measurements were performed in a two-electrode system using a rectangular quartz beaker as a reactor. The prepared FTO@BiOCl electrode was used as a photoanode in the system, while a platinum wire served as the counter electrode. The quartz reactor was filled with a 0.1 M Na$_2$SO$_4$ aqueous solution as the electrolyte. The electrochemical measurements were conducted with an Autolab Potentiostat PGSTAT128N (Utrecht, Netherlands). A 100 W xenon-ozone lamp was employed as the solar simulator.

3.6. Chemical Analysis

The determination of LOS was conducted using high-performance liquid chromatography (HPLC) with a photodiode array detector (PDA) (Waters Alliance 2695, Milford, MA, USA). The HPLC system was equipped with a C18 reverse-phase column (Kinetex XB-C18, 2100 μm; 2.6 mm internal diameter × 50 mm length) (Milford, MA, USA). An isocratic elution program involving 0.1% H$_3$PO$_4$ (60%) and acetonitrile (40%) with a flow rate equal to 0.2 mL/min was employed. Samples were filtered and injected into the column using a full-loop injection of 100 μL, and the PDA was set at a wavelength of 220 nm. TOC was measured using a TOC analyzer (TOC-L, Company: Shimadzu, JAPAN).

4. Conclusions

This work focused on the synthesis, characterization, and application of BiOCl to decompose Losartan under laboratory or pilot-plant conditions using simulated and natural solar light. BiOCl was synthesized using a relatively simple technique, and according to the results, demonstrated response and photocatalytic activity expressed as LOS removal in the visible part of the solar spectrum. The examined system was capable of eliminating LOS in short treatment times (less than 30 min). The material exhibited high stability regarding produced photocurrent and retained 100% LOS removal after five sequential experiments. Photogenerated holes, superoxide radicals produced from photogenerated electrons, and singlet oxygen were the main reactive species dictating Losartan's decomposition. The process performance was strongly affected by pH, with significant retardation observed in alkaline conditions and in real matrices due to competition for both reactive species and adsorption on the catalyst, highlighting the need for the evaluation of photocatalytic systems in representative conditions. Experiments conducted in a stainless-steel flat-plate reactor demonstrated the efficiency of the process at the pilot- scale; however, additional research is needed for the implementation of photocatalytic pilot-plants for specific purposes such as tertiary treatment or the treatment of hospital or pharmaceutical wastewaters, and the optimization of pilot-plants under actual conditions.

Author Contributions: Conceptualization, A.P. and Z.F.; methodology, A.P., M.S. and Z.F.; formal analysis, K.K., A.P., A.A.I. and Z.F.; investigation, K.K. and A.A.I. resources, M.S. and Z.F.; data curation, A.A.I., A.P., K.K., M.S. and Z.F.; writing—original draft preparation, K.K., A.A.I. and A.P. writing—review and editing, K.K., A.A.I., A.P., M.S. and Z.F.; visualization, K.K., A.A.I. and A.P.;

References

1. Mukhopadhyay, A.; Duttagupta, S.; Mukherjee, A. Emerging Organic Contaminants in Global Community Drinking Water Sources and Supply: A Review of Occurrence, Processes and Remediation. *J. Environ. Chem. Eng.* **2022**, *10*, 107560. [CrossRef]
2. Tufail, A.; Price, W.E.; Mohseni, M.; Pramanik, B.K.; Hai, F.I. A Critical Review of Advanced Oxidation Processes for Emerging Trace Organic Contaminant Degradation: Mechanisms, Factors, Degradation Products, and Effluent Toxicity. *J. Water Process Eng.* **2021**, *40*, 101778. [CrossRef]
3. Wang, J.; Wang, S. Reactive Species in Advanced Oxidation Processes: Formation, Identification and Reaction Mechanism. *Chem. Eng. J.* **2020**, *401*, 126158. [CrossRef]
4. Saravanan, A.; Deivayanai, V.C.; Kumar, P.S.; Rangasamy, G.; Hemavathy, R.V.; Harshana, T.; Gayathri, N.; Alagumalai, K. A Detailed Review on Advanced Oxidation Process in Treatment of Wastewater: Mechanism, Challenges and Future Outlook. *Chemosphere* **2022**, *308*, 136524. [CrossRef]
5. Kouvelis, K.; Kampioti, A.A.; Petala, A.; Frontistis, Z. Degradation of Sulfamethoxazole Using a Hybrid CuOx-BiVO$_4$/SPS/Solar System. *Catalysts* **2022**, *12*, 882. [CrossRef]
6. Fedorov, K.; Dinesh, K.; Sun, X.; Darvishi Cheshmeh Soltani, R.; Wang, Z.; Sonawane, S.; Boczkaj, G. Synergistic Effects of Hybrid Advanced Oxidation Processes (AOPs) Based on Hydrodynamic Cavitation Phenomenon—A Review. *Chem. Eng. J.* **2022**, *432*, 134191. [CrossRef]
7. Antoniadou, M.; Falara, P.P.; Likodimos, V. Photocatalytic Degradation of Pharmaceuticals and Organic Contaminants of Emerging Concern Using Nanotubular Structures. *Curr. Opin. Green Sustain. Chem.* **2021**, *29*, 100470. [CrossRef]
8. Loeb, S.K.; Alvarez, P.J.J.; Brame, J.A.; Cates, E.L.; Choi, W.; Crittenden, J.; Dionysiou, D.D.; Li, Q.; Li-Puma, G.; Quan, X.; et al. The Technology Horizon for Photocatalytic Water Treatment: Sunrise or Sunset? *Environ. Sci. Technol.* **2019**, *53*, 2937–2947. [CrossRef] [PubMed]
9. Fernandes, A.; Makoś, P.; Wang, Z.; Boczkaj, G. Synergistic Effect of TiO2 Photocatalytic Advanced Oxidation Processes in the Treatment of Refinery Effluents. *Chem. Eng. J.* **2020**, *391*, 123488. [CrossRef]
10. Fernandes, A.; Gągol, M.; Makoś, P.; Khan, J.A.; Boczkaj, G. Integrated Photocatalytic Advanced Oxidation System (TiO$_2$/UV/O$_3$/H$_2$O$_2$) for Degradation of Volatile Organic Compounds. *Sep. Purif. Technol.* **2019**, *224*, 1–14. [CrossRef]
11. Khan, J.A.; Sayed, M.; Shah, N.S.; Khan, S.; Zhang, Y.; Boczkaj, G.; Khan, H.M.; Dionysiou, D.D. Synthesis of Eosin Modified TiO2 Film with Co-Exposed {001} and {101} Facets for Photocatalytic Degradation of Para-Aminobenzoic Acid and Solar H$_2$ Production. *Appl. Catal. B Environ.* **2020**, *265*, 118557. [CrossRef]
12. Monfort, O.; Pop, L.C.; Sfaelou, S.; Plecenik, T.; Roch, T.; Dracopoulos, V.; Stathatos, E.; Plesch, G.; Lianos, P. Photoelectrocatalytic Hydrogen Production by Water Splitting Using BiVO4 Photoanodes. *Chem. Eng. J.* **2016**, *286*, 91–97. [CrossRef]
13. Huang, C.; Chen, L.; Li, H.; Mu, Y.; Yang, Z. Synthesis and Application of Bi2WO6 for the Photocatalytic Degradation of Two Typical Fluoroquinolones under Visible Light Irradiation. *RSC Adv.* **2019**, *9*, 27768–27779. [CrossRef] [PubMed]
14. Sajjad, S.; Leghari, S.A.K.; Zhang, J. Nonstoichiometric Bi$_2$O$_3$: Efficient Visible Light Photocatalyst. *RSC Adv.* **2013**, *3*, 1363–1367. [CrossRef]
15. Landge, V.K.; Sonawane, S.H.; Sivakumar, M.; Sonawane, S.S.; Uday Bhaskar Babu, G.; Boczkaj, G. S-Scheme Heterojunction Bi$_2$O$_3$-ZnO/Bentonite Clay Composite with Enhanced Photocatalytic Performance. *Sustain. Energy Technol. Assess.* **2021**, *45*, 101194. [CrossRef]
16. Zhang, K.; Zhang, Y.; Zhang, D.; Liu, C.; Zhou, X.; Yang, H.; Qu, J.; He, D. Efficient Photocatalytic Water Disinfection by a Novel BP/BiOBr S-Scheme Heterojunction Photocatalyst. *Chem. Eng. J.* **2023**, *468*, 143581. [CrossRef]
17. Amirulsyafiee, A.; Khan, M.M.; Harunsani, M.H. Ag$_3$PO$_4$ and Ag$_3$PO$_4$–Based Visible Light Active Photocatalysts: Recent Progress, Synthesis, and Photocatalytic Applications. *Catal. Commun.* **2022**, *172*, 106556. [CrossRef]
18. Li, M.; Sun, J.; Chen, G.; Wang, S.; Yao, S. Inducing Photocarrier Separation via 3D Porous Faveolate Cross-Linked Carbon to Enhance Photothermal/Pyroelectric Property. *Adv. Powder Mater.* **2022**, *1*, 100032. [CrossRef]

19. Song, S.; Xing, Z.; Zhao, H.; Li, Z.; Zhou, W. Recent Advances in Bismuth-Based Photocatalysts: Environment and Energy Applications. *Green Energy Environ.* 2022; *in press*. [CrossRef]

20. Gao, X.; Guo, Q.; Tang, G.; Zhu, W.; Yang, X.; Luo, Y. TBAOH Assisted Synthesis of Ultrathin BiOCl Nanosheets with Enhanced Charge Separation Efficiency for Superior Photocatalytic Activity in Carbamazepine Degradation. *J. Colloid Interface Sci.* **2020**, *570*, 242–250. [CrossRef]

21. Zhang, J.; Wang, Z.; Fan, M.; Tong, P.; Sun, J.; Dong, S.; Sun, J. Ultra-Light and Compressible 3D BiOCl/RGO Aerogel with Enriched Synergistic Effect of Adsorption and Photocatalytic Degradation of Oxytetracycline. *J. Mater. Res. Technol.* **2019**, *8*, 4577–4587. [CrossRef]

22. Shahid, M.Z.; Mehmood, R.; Athar, M.; Hussain, J.; Wei, Y.; Khaliq, A. BiOCl Nanoplates Doped with Fe^{3+} Ions for the Visible-Light Degradation of Aqueous Pollutants. *ACS Appl. Nano Mater.* **2021**, *4*, 746–758. [CrossRef]

23. Petala, A.; Arvaniti, O.S.; Travlou, G.; Mantzavinos, D.; Frontistis, Z. Solar Light Induced Photocatalytic Removal of Sulfamethoxazole from Water and Wastewater Using BiOCl Photocatalyst. *J. Environ. Sci. Health Part A* **2021**, *56*, 963–972. [CrossRef] [PubMed]

24. Grilla, E.; Kagialari, M.N.; Petala, A.; Frontistis, Z.; Mantzavinos, D. Photocatalytic Degradation of Valsartan by MoS_2/BiOCl Heterojunctions. *Catalysts* **2021**, *11*, 650. [CrossRef]

25. Galani, A.; Alygizakis, N.; Aalizadeh, R.; Kastritis, E.; Dimopoulos, M.-A.; Thomaidis, N.S. Patterns of Pharmaceuticals Use during the First Wave of COVID-19 Pandemic in Athens, Greece as Revealed by Wastewater-Based Epidemiology. *Sci. Total Environ.* **2021**, *798*, 149014. [CrossRef]

26. Salazar, C.; Contreras, N.; Mansilla, H.D.; Yáñez, J.; Salazar, R. Electrochemical Degradation of the Antihypertensive Losartan in Aqueous Medium by Electro-Oxidation with Boron-Doped Diamond Electrode. *J. Hazard. Mater.* **2016**, *319*, 84–92. [CrossRef]

27. Ioannidi, A.; Arvaniti, O.S.; Nika, M.-C.; Aalizadeh, R.; Thomaidis, N.S.; Mantzavinos, D.; Frontistis, Z. Removal of Drug Losartan in Environmental Aquatic Matrices by Heat-Activated Persulfate: Kinetics, Transformation Products and Synergistic Effects. *Chemosphere* **2022**, *287*, 131952. [CrossRef]

28. de Andrade, J.R.; Vieira, M.G.A.; da Silva, M.G.C.; Wang, S. Oxidative Degradation of Pharmaceutical Losartan Potassium with N-Doped Hierarchical Porous Carbon and Peroxymonosulfate. *Chem. Eng. J.* **2020**, *382*, 122971. [CrossRef]

29. Guateque-Londoño, J.F.; Serna-Galvis, E.A.; Silva-Agredo, J.; Ávila-Torres, Y.; Torres-Palma, R.A. Dataset on the Degradation of Losartan by TiO(2)-Photocatalysis and UVC/Persulfate Processes. *Data Br.* **2020**, *31*, 105692. [CrossRef]

30. Gao, X.; Guo, Q.; Tang, G.; Zhu, W.; Luo, Y. Controllable Synthesis of Solar-Light-Driven BiOCl Nanostructures for Highly Efficient Photocatalytic Degradation of Carbamazepine. *J. Solid State Chem.* **2019**, *277*, 133–138. [CrossRef]

31. Gao, X.; Zhang, X.; Wang, Y.; Peng, S.; Yue, B.; Fan, C. Photocatalytic Degradation of Carbamazepine Using Hierarchical BiOCl Microspheres: Some Key Operating Parameters, Degradation Intermediates and Reaction Pathway. *Chem. Eng. J.* **2015**, *273*, 156–165. [CrossRef]

32. Shen, T.; Shi, X.; Guo, J.; Li, J.; Yuan, S. Photocatalytic Removal of NO by Light-Driven Mn3O4/BiOCl Heterojunction Photocatalyst: Optimization and Mechanism. *Chem. Eng. J.* **2021**, *408*, 128014. [CrossRef]

33. Akhter, P.; Nawaz, S.; Shafiq, I.; Nazir, A.; Shafique, S.; Jamil, F.; Park, Y.K.; Hussain, M. Efficient Visible Light Assisted Photocatalysis Using ZnO/TiO_2 Nanocomposites. *Mol. Catal.* **2023**, *535*, 112896. [CrossRef]

34. Spasiano, D.; Marotta, R.; Malato, S.; Fernandez-Ibañez, P.; Di Somma, I. Solar Photocatalysis: Materials, Reactors, Some Commercial, and Pre-Industrialized Applications. A Comprehensive Approach. *Appl. Catal. B Environ.* **2015**, *170–171*, 90–123. [CrossRef]

35. Kollipara, S.; Bende, G.; Bansal, Y.; Saha, R. Stability-Indicating Reversed-Phase Liquid Chromatographic Method for Simultaneous Determination of Losartan Potassium and Ramipril in Tablets. *Indian J. Pharm. Sci.* **2012**, *74*, 201–210. [CrossRef] [PubMed]

36. Sapińska, D.; Adamek, E.; Masternak, E.; Zielińska-Danch, W.; Baran, W. Influence of PH on the Kinetics and Products of Photocatalytic Degradation of Sulfonamides in Aqueous Solutions. *Toxics* **2022**, *10*, 655. [CrossRef]

37. Puscedu, F.H.; Guimarães, M.M.; Lopes, L.O.; Souza, L.S.; Cortez, F.S.; Pereira, C.D.S.; Choueri, R.B.; Cesar, A. Biological Effects of the Antihypertensive Losartan under Different Ocean Acidification Scenarios. *Environ. Pollut.* **2022**, *292*, 118329. [CrossRef]

38. Rioja, N.; Zorita, S.; Peñas, F.J. Effect of Water Matrix on Photocatalytic Degradation and General Kinetic Modeling. *Appl. Catal. B Environ.* **2016**, *180*, 330–335. [CrossRef]

39. Barbosa, M.O.; Moreira, N.F.F.; Ribeiro, A.R.; Pereira, M.F.R.; Silva, A.M.T. Occurrence and Removal of Organic Micropollutants: An Overview of the Watch List of EU Decision 2015/495. *Water Res.* **2016**, *94*, 257–279. [CrossRef]

40. Duta, A.; Malato, S.; Bogatu, C.; Covei, M.; Polo-l, M.I. Novel ZnO Photocatalysts for Pollutants' Abatement under Solar Radiation at Pilot Plant Scale. *Catal. Today* **2023**, *415*, 113947. [CrossRef]

41. Gao, L.; Zhou, B.; Wang, F.; Yuan, R.; Chen, H.; Han, X. Effect of Dissolved Organic Matters and Inorganic Ions on TiO_2 Photocatalysis of Diclofenac: Mechanistic Study and Degradation Pathways. *Environ. Sci. Pollut. Res.* **2020**, *27*, 2044–2053. [CrossRef]

42. Metheniti, M.; Frontistis, Z.; Ribeiro, R.; Silva, A.; Faria, J.; Gomes, H.; Mantzavinos, D. Degradation of Propyl Paraben by Activated Persulfate Using Iron-Containing Magnetic Carbon Xerogels: Investigation of Water Matrix and Process Synergy Effects. *Environ. Sci. Pollut. Res.* **2018**, *25*, 34801–34810. [CrossRef] [PubMed]

43. Lai, W.W.P.; Hsu, M.H.; Lin, A.Y.C. The Role of Bicarbonate Anions in Methotrexate Degradation via UV/TiO$_2$: Mechanisms, Reactivity and Increased Toxicity. *Water Res.* **2017**, *112*, 157–166. [CrossRef] [PubMed]

44. Li, X.; Chen, Y.; Tao, Y.; Shen, L.; Xu, Z.; Bian, Z.; Li, H. Challenges of Photocatalysis and Their Coping Strategies. *Chem Catal.* **2022**, *2*, 1315–1345. [CrossRef]

45. Petala, A.; Tsikritzis, D.; Kollia, M.; Ladas, S.; Kennou, S.; Kondarides, D.I. Synthesis and Characterization of N-Doped TiO$_2$ Photocatalysts with Tunable Response to Solar Radiation. *Appl. Surf. Sci.* **2014**, *305*, 281–291. [CrossRef]

46. Sarwan, B.; Pare, B.; Acharya, A.D.; Jonnalagadda, S.B. Mineralization and Toxicity Reduction of Textile Dye Neutral Red in Aqueous Phase Using BiOCl Photocatalysis. *J. Photochem. Photobiol. B Biol.* **2012**, *116*, 48–55. [CrossRef]

47. Schneider, T.; Peralta-zamora, P.; Firak, D.S.; Ribeiro, R.R. Use of Scavenger Agents in Heterogeneous Photocatalysis: Truths, Half-Truths, and Misinterpretations. *Phys. Chem. Chem. Phys.* **2020**, *22*, 15723–15733. [CrossRef]

48. Bancirova, M. Sodium Azide as a Specific Quencher of Singlet Oxygen during Chemiluminescent Detection by Luminol and Cypridina Luciferin Analogues. *Luminescence* **2011**, *26*, 685–688. [CrossRef]

49. Yang, B.J.; Luo, W.; Liao, Q.; Zhu, J.Y.; Gan, M.; Liu, X.D.; Qiu, G.Z. Photogenerated-Hole Scavenger for Enhancing Photocatalytic Chalcopyrite Bioleaching. *Trans. Nonferrous Met. Soc. China* **2020**, *30*, 200–211. [CrossRef]

50. Nosaka, Y.; Nosaka, A.Y. Comment on "Singlet Oxygen ^{1}O$_2$ in Photocatalysis on TiO$_2$. *Where Does It Come From?" J. Phys. Chem. C* **2019**, *123*, 27993–27995. [CrossRef]

51. Barrios, B.; Mohrhardt, B.; Doskey, P.V.; Minakata, D. Mechanistic Insight into the Reactivities of Aqueous-Phase Singlet Oxygen with Organic Compounds. *Environ. Sci. Technol.* **2021**, *55*, 8054–8067. [CrossRef] [PubMed]

52. Ioannidi, A.A.; Zappa, J.; Petala, A.; Souliotis, M.; Mantzavinos, D.; Frontistis, Z. Solar Light-Induced Photocatalytic Degradation of Sulfamethoxazole by Cobalt Phosphide-Promoted Bismuth Vanadate. *Water* **2023**, *15*, 1370. [CrossRef]

53. Malato, S.; Maldonado, M.I.; Fernández-Ibáñez, P.; Oller, I.; Polo, I.; Sánchez-Moreno, R. Decontamination and Disinfection of Water by Solar Photocatalysis: The Pilot Plants of the Plataforma Solar de Almeria. *Mater. Sci. Semicond. Process.* **2016**, *42*, 15–23. [CrossRef]

54. Hou, J.; Dai, D.; Wei, R.; Wu, X.; Wang, X.; Tahir, M.; Zou, J.-J. Narrowing the Band Gap of BiOCl for the Hydroxyl Radical Generation of Photocatalysis under Visible Light. *ACS Sustain. Chem. Eng.* **2019**, *7*, 16569–16576. [CrossRef]

55. Yahia, I.S.; Jilani, A.; Abdel-wahab, M.S.; Zahran, H.Y. Optik The Photocatalytic Activity of Graphene Oxide/Ag$_3$PO$_4$ Nano-Composite: Loading Effect. *Optik* **2016**, *127*, 10746–10757. [CrossRef]

56. Tauc, J.; Grigorovici, R.; Vancu, A. Optical Properties and Electronic Structure of Amorphous Germanium. *Phys. Status Solidi* **1966**, *15*, 627–637. [CrossRef]

57. Ganesh, V.; Ravi Kumar, B.; AlAbdulaal, T.H.; Yahia, I.S.; Abdel-wahab, M.S.; Ade, R.; Hussien, M.S.A.; Keshway, M. Electrocatalytic Degradation of Rhodamine B Using Li-Doped ZnO Nanoparticles: Novel Approach. *Materials* **2023**, *16*, 1177. [CrossRef]

58. Abdel-wahab, M.S. Substrate Temperature Impact on the Structural, Optical and Photo-Catalytic Activity of Sputtered Cu-Doped ZnO Thin Films. *J. Electron. Mater.* **2021**, *50*, 4364–4372. [CrossRef]

59. Wang, J.; Wei, Y.; Yang, B.; Wang, B.; Chen, J.; Jing, H. In Situ Grown Heterojunction of Bi$_2$WO$_6$/BiOCl for Efficient Photoelectrocatalytic CO$_2$ Reduction. *J. Catal.* **2019**, *377*, 209–217. [CrossRef]